View metadata, citation and similar papers at core.ac.uk
brought to you by CORE
provided by ScholarWorks@UNIST

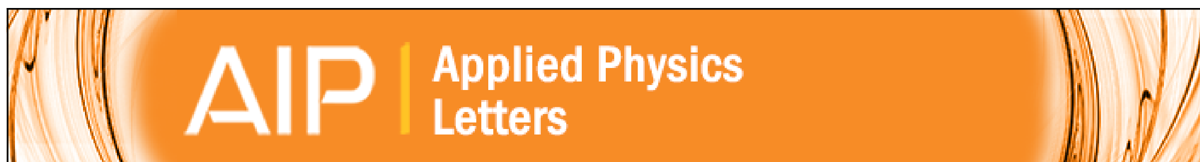

Experimental investigation of plasmofluidic waveguides

Bonwoo Ku, Jin-Soo Shin, and Min-Suk Kwon

Citation: Applied Physics Letters **107**, 201104 (2015); doi: 10.1063/1.4935984
View online: http://dx.doi.org/10.1063/1.4935984
View Table of Contents: http://scitation.aip.org/content/aip/journal/apl/107/20?ver=pdfcov
Published by the AIP Publishing

Articles you may be interested in
A highly efficient surface plasmon polaritons excitation achieved with a metal-coupled metal-insulator-metal waveguide
AIP Advances **4**, 127114 (2014); 10.1063/1.4903775

Low-loss waveguiding and detecting structure for surface plasmon polaritons
Appl. Phys. Lett. **104**, 081111 (2014); 10.1063/1.4866792

Zener tunneling in plasmonic metal gap waveguide superlattices
Appl. Phys. Lett. **93**, 133118 (2008); 10.1063/1.2995865

Dielectric-loaded surface plasmon-polariton waveguides at telecommunication wavelengths: Excitation and characterization
Appl. Phys. Lett. **92**, 011124 (2008); 10.1063/1.2825588

Air gaps in metal stripe waveguides supporting long-range surface plasmon polaritons
J. Appl. Phys. **102**, 033112 (2007); 10.1063/1.2764222

AIP Applied Physics Reviews
NEW Special Topic Sections
NOW ONLINE
Lithium Niobate Properties and Applications: Reviews of Emerging Trends
AIP Applied Physics Reviews

This article is copyrighted as indicated in the article. Reuse of AIP content is subject to the terms at: http://scitation.aip.org/termsconditions. Downloaded to IP: 114.70.7.203 On: Wed, 16 Dec 2015 01:14:20

Experimental investigation of plasmofluidic waveguides

Bonwoo Ku,[1] Jin-Soo Shin,[2] and Min-Suk Kwon[1,a)]
[1]School of Electrical and Computer Engineering, UNIST, 50 UNIST-gil, Eonyang-eup, Ulju-gun, Ulsan 689-798, South Korea
[2]Department of Electrical Engineering, KAIST, 291 Daehak-ro, Yuseong-gu, Daejeon 305-701, South Korea

(Received 14 July 2015; accepted 5 November 2015; published online 16 November 2015)

Plasmofluidic waveguides are based on guiding light which is strongly confined in fluid with the assistance of a surface plasmon polariton. To realize plasmofluidic waveguides, metal-insulator-silicon-insulator-metal (MISIM) waveguides, which are hybrid plasmonic waveguides fabricated using standard complementary metal-oxide-semiconductor technology, are employed. The insulator of the MISIM waveguide is removed to form 30-nm-wide channels, and they are filled with fluid. The plasmofluidic waveguide has a subwavelength-scale mode area since its mode is strongly confined in the fluid. The waveguides are experimentally characterized for different fluids. When the refractive index of the fluid is 1.440, the plasmofluidic waveguide with 190-nm-wide silicon has propagation loss of 0.46 dB/μm; the coupling loss between it and an ordinary silicon photonic waveguide is 1.79 dB. The propagation and coupling losses may be reduced if a few fabrication-induced imperfections are removed. The plasmofluidic waveguide may pave the way to a dynamically phase-tunable ultracompact device. © *2015 Author(s). All article content, except where otherwise noted, is licensed under a Creative Commons Attribution 3.0 Unported License.*
[http://dx.doi.org/10.1063/1.4935984]

Nanoplasmonic waveguides are based on metal which enables a surface plasmon polariton (SPP) to exist around a metal-dielectric interface. Since they support waveguide modes which are confined in a region with dimensions smaller than the diffraction limit, they can be used to implement highly integrated optoelectronic devices.[1–4] For this reason, they have attracted a lot of attention for more than a decade. While a plethora of nanoplasmonic waveguides have been studied, silicon-based hybrid plasmonic waveguides are prominent.[5–12] This is because they are compatible with conventional silicon photonic devices and their modes can have both subwavelength-scale mode area and relatively small propagation loss. Metal-insulator-silicon-insulator-metal (MISIM) waveguides are such hybrid plasmonic waveguides which are realized by using standard complementary metal-oxide-semiconductor (CMOS) technology.[13–24]

A variety of passive MISIM waveguide devices have been realized.[18–20,23,24] For active MISIM waveguide devices, it was experimentally demonstrated that the phase of the MISIM waveguide mode can be tuned by depleting or accumulating electrons in the silicon strip of a MISIM waveguide.[21] This method changes not only the phase but also the propagation loss of the MISIM waveguide mode. To change mainly the phase, a different method is required. Obviously, tuning the refractive index of the insulator of a MISIM waveguide corresponds to such a method since the MISIM waveguide mode is strongly confined in the insulator. Therefore, it is indispensable to effectively control the refractive index of the insulator.

A large change of the refractive index of the insulator is achievable if the insulator is dynamically replaced by another insulator. This is possible when the insulator is fluid. The insulator of the MISIM waveguide, which we have been studying, is not covered by metal.[22–24] Hence, it can be removed such that very narrow channels of width 30 nm remain to be filled with fluid. Since this MISIM waveguide mode is substantially confined in the fluid, the interaction between light and the fluid is significantly enhanced. This character is similar to that of optofluidic waveguides,[25] and this MISIM waveguide is a combination of nanoplasmonic and optofluidic waveguides. In this sense, it is hereafter called a plasmofluidic waveguide. In this paper, the straight plasmofluidic waveguides are experimentally investigated. Compared to a previous plasmofluidic waveguide based on a long range SPP,[26] this plasmofluidic waveguide possesses mode area smaller than the diffraction limit. For various fluids, the propagation loss of the plasmofluidic waveguide and the coupling loss between the plasmofluidic waveguide and a silicon photonic waveguide are explained and compared with those calculated theoretically. In addition, the operation of the plasmofluidic waveguide with liquid crystal (LC) used as the fluid is discussed.

The structure of the plasmofluidic waveguide is almost the same as that of our previous MISIM waveguide except that the insulator (silicon dioxide, SiO_2) and thin silicon nitride layer of the latter do not exist in the former. The top view of the structure investigated for the plasmofluidic waveguide is schematically shown in Fig. 1(a). The plasmofluidic waveguide of length l_P is connected to the silicon (Si) photonic waveguides with a 450-nm-wide core via the tapering regions of length 600 nm. The cross-sectional structures of the plasmofluidic waveguide and the Si photonic waveguide are shown in Figs. 1(b) and 1(c), respectively. The plasmofluidic waveguide consists of the 250-nm-thick Si strip of width w_S and the 260-nm-thick copper (Cu) patterns laterally sandwiching the Si strip with the 30-nm-wide channels in between. The Cu patterns are recessed by 30 nm from the bottom of the Si strip. Fluid of refractive index n_l fills the

a)Electronic mail: mskwon@unist.ac.kr

 © Author(s) 2015

This article is copyrighted as indicated in the article. Reuse of AIP content is subject to the terms at: http://scitation.aip.org/termsconditions. Downloaded to IP: 114.70.7.203 On: Wed, 16 Dec 2015 01:14:20

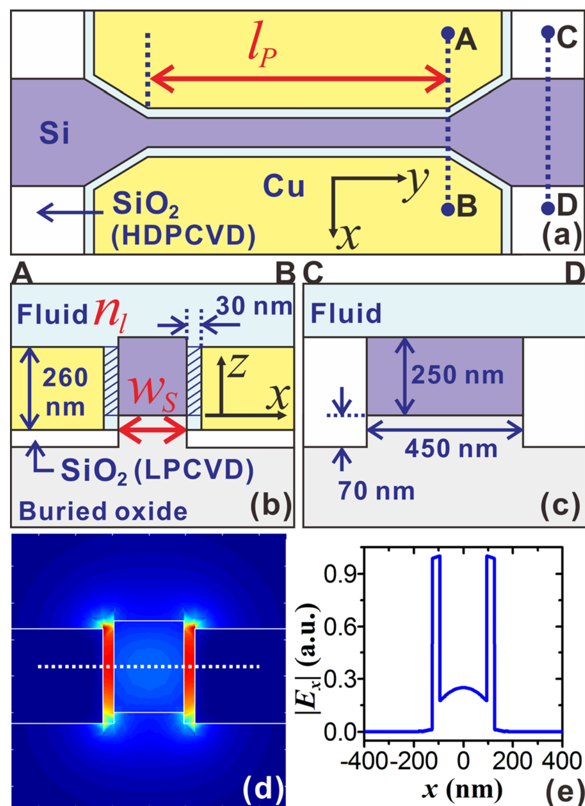

FIG. 1. (a) Schematic diagram of the structure investigated for the plasmofluidic waveguide. Cross-sectional structures of (b) the plasmofluidic waveguide and (c) the Si photonic waveguide with the 450-nm-wide core. (d) Distribution of $|\mathbf{E}|$ for $w_S = 190$ nm and $n_l = 1.44$ in the xz-plane. (e) Distribution of $|E_x|$ along the dotted line at $z = 125$ nm.

channels and covers the structure. A 30-μm-wide microfluidic channel made of SU-8, which is not shown in Fig. 1(a), is placed perpendicular to the plasmofluidic waveguide. Hence, the Si photonic waveguides in the microfluidic channel are covered by the fluid, but those outside the microfluidic channel are covered by SU-8. Actually, the SU-8 pattern for the microfluidic channel is essential to realize the structure for the plasmofluidic waveguide as explained below.

When $w_S \leq 230$ nm, the plasmofluidic waveguide supports just one guided mode called a hybrid plasmonic mode. The hybrid plasmonic mode has a dominant electric field component E_x in the x axis. The calculated distribution of the electric field $\mathbf{E}$ for $w_S = 190$ nm and $n_l = 1.44$ is shown in Fig. 1(d), and the distribution of $|E_x|$ in the middle of the plasmofluidic waveguide (i.e., at $z = 125$ nm) is shown in Fig. 1(e). For the calculation, a commercial mode solver based on the finite element method (FIMMWAVE, Photon Design) was used. In addition, the dielectric constant of Cu as a function of the free-space wavelength λ was interpolated from the measured values in Ref. 27 and it was used for all the following simulations of the plasmofluidic waveguide. It is $-122 + i3.83$ at $\lambda = 1550$ nm, and the refractive indices of Si and SiO_2 are 3.485 and 1.445, respectively. The electric field is highly enhanced at the metal-fluid interface due to the existence of an SPP and at the fluid-Si interface due to the discontinuity of a surface-normal electric field component. The mode area of the hybrid plasmonic mode, which was calculated in the same way as in Ref. 22, is $2.98 \times 10^{-2}\,\mu m^2 = 0.103 \times [\lambda/(2n_l)]^2$. The fractional power which the hybrid plasmonic mode transports through the hatched regions in the channels is 37%. The mode area and the fractional power do not change significantly as n_l changes.

The fabrication of the plasmofluidic waveguide starts from that of the MISIM waveguide. The process of fabricating the MISIM waveguide is the same as in Refs. 23 and 24, which is based on standard CMOS technology, including 248 nm optical lithography, dry etching, high-density plasma chemical vapor deposition (HDPCVD), low pressure chemical vapor deposition (LPCVD), chemical mechanical polishing (CMP), etc. Identical chips with the MISIM waveguides, which have dimensions of 20 mm × 15 mm, were made on an 8-in. silicon-on-insulator wafer. One chip was diced out of the wafer, and the SU-8 microfluidic channel was formed on it by patterning SU-8 (MicroChem, SU-8 2015). Then, the insulator made by LPCVD was etched away with the SU-8 pattern used as an etching mask. To minimize the etching-induced losses of the Si photonic waveguides on the chip, it is imperative to protect them with the SU-8 pattern from being affected by the etching. Previously, a mixture of buffered oxide etch (BOE) solution (Model 1178–03, JT Baker) and glycerol with a weight ratio of 2:1 had been employed for the etching to reduce Cu corrosion.[23] However, it was found that quick etching with only the BOE solution is better for the properties of the plasmofluidic waveguides than slow etching with the mixture. Hence, the chip was immersed into the BOE solution for 55 s, thoroughly rinsed with deionized water, and dried. Finally, the chip was diced to make the input and output facets of Si photonic waveguides with a 5-μm-wide core, which are connected to the 450-nm-core waveguides through 200-μm-long tapering regions. During the dicing, the SU-8 pattern again plays the important role of reducing dicing-induced damage to the Si photonic waveguides.

A scanning electron microscope (SEM) image of the fabricated structure for the plasmofluidic waveguide is shown in Fig. 2(a); an enlarged image of the tapering region between the 450-nm-core waveguide and the plasmofluidic waveguide is shown in Fig. 2(b); an SEM image of the cross-section of the plasmofluidic waveguide is shown in Fig. 2(c). The bumpy band observed at the end of the 450-nm-core waveguide in Fig. 2(b) was examined to be residual Si oxide. As shown in Fig. 2(c), the insulator beneath the Cu patterns is slightly etched away. Since the etching time is short, such undercuts are not well controllable. Actually, there was another chip without the undercuts. The influence of the undercuts on the characteristics of the hybrid plasmonic mode is weak, and the structure without the undercuts in Fig. 1(b) was considered in the following simulations.

For measurement, light from a tunable laser was horizontally polarized and launched into the input 5-μm-core waveguide via a lensed fiber. The wavelength of the light was set to 1550 nm. The light exiting from the output 5-μm-core waveguide was coupled to another lensed fiber connected to a photodetector. For reference, we measured the fiber-to-fiber insertion loss (in dB) of only the 4-mm-long, 450-nm-core waveguide connected to the input and output 5-μm-core waveguides. The length of the 450-nm-core

This article is copyrighted as indicated in the article. Reuse of AIP content is subject to the terms at: http://scitation.aip.org/termsconditions. Downloaded to IP: 114.70.7.203 On: Wed, 16 Dec 2015 01:14:20

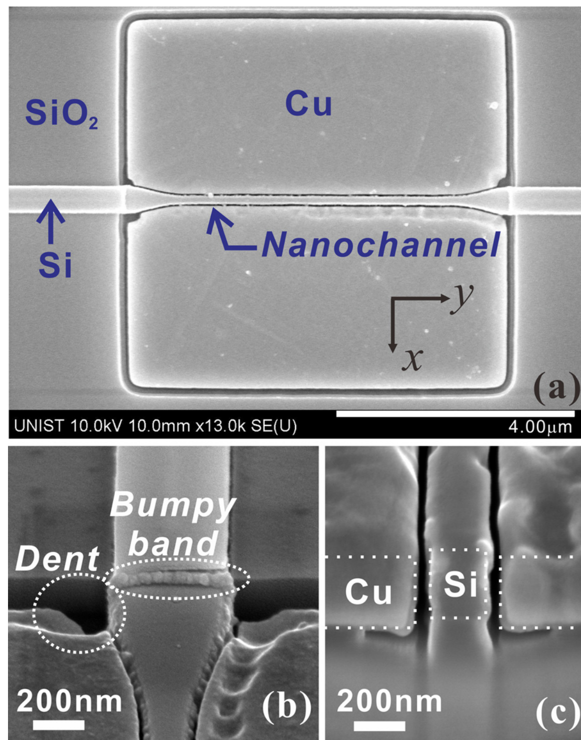

FIG. 2. (a) Surface SEM image of the fabricated structure investigated for the plasmofluidic waveguide. (b) Enlarged SEM image of the tapering region. The bumpy band, which was examined to be residual oxide, and the dent at the corner of the Cu pattern are fabrication imperfections. They may affect the coupling loss between the plasmofluidic and Si photonic waveguides. (c) Enlarged image of the cross-section of the plasmofluidic waveguide. The dotted boxes show the Cu pattern and the Si strip.

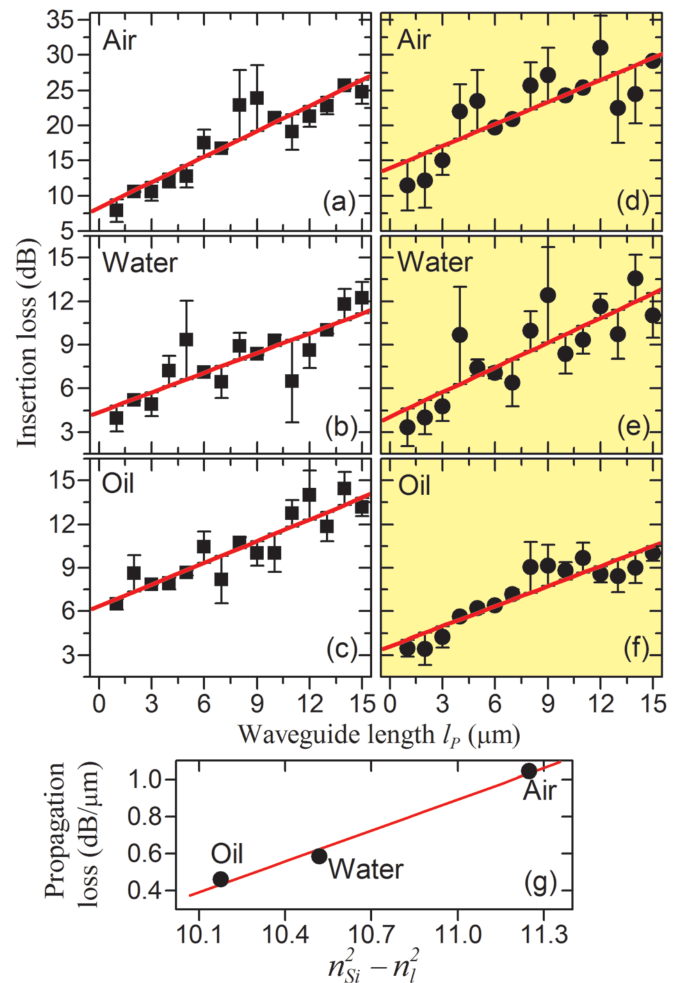

FIG. 3. Relations of the insertion loss of the plasmofluidic waveguide to the waveguide length l_P. (a)–(c) are those for $w_S = 160$ nm. (d)–(f) are those for $w_S = 190$ nm. The symbols represent the measured values, and the straight lines are fitted to the measured values. (g) Relation of the propagation loss to $(n_{Si}^2 - n_l^2)$ for $w_S = 190$ nm. The symbols represent the measured values, and the straight line is fitted to the measured values.

waveguide is the same as the total length of the two 450-nm-core waveguides connected to the plasmofluidic waveguide. We subtracted the reference value from the fiber-to-fiber insertion loss (in dB) of the structure for the plasmofluidic waveguide. The resultant value is hereafter called the insertion loss of the plasmofluidic waveguide.

For various values of w_S and n_l, the relations of the insertion loss to l_P are shown in Fig. 3. Here, w_S is either 160 or 190 nm. When the fluid is air, water, and index oil, n_l is 1, 1.311, and 1.440, respectively. Each insertion loss for a value of l_P is the average of those of the five plasmofluidic waveguides with the same value of l_P. The error bar corresponds to the standard deviation of the five insertion losses. A straight line is fitted to each relation. The relation of the insertion loss to l_P fluctuates around the straight line partly due to the Fabry-Perot resonance of the 15-mm-long chip itself.[23] The slope of the straight line is the propagation loss of the plasmofluidic waveguide, and the y-intercept of the straight line corresponds to two times the coupling loss of the tapering region.

The measured and calculated values of the propagation loss and those of the coupling loss are summarized in Table I. The propagation loss was calculated by using FIMMWAVE, and the coupling loss was calculated by using the finite difference time domain (FDTD) method (FDTD Solutions, Lumerical). On the whole, the propagation loss for $w_S = 190$ nm is smaller than that for $w_S = 160$ nm. Similar to the previous observation,[23] this is caused by the fact that the narrower the Si strip is, the more strongly the hybrid plasmonic mode is confined in the channels. As n_l increases, the propagation loss decreases. However, we observed that the propagation loss does not change significantly when n_l increases from 1.440 to 1.53. Although the measured propagation loss of the MISIM waveguide before removing the insulator is close to the calculated one, the measured propagation loss of the plasmofluidic waveguide is larger than the calculated one. The difference between the measured and calculated propagation losses may be caused by roughness which is considered to arise on the sidewalls of the Si strip from etching the insulator. Actually, we observed

TABLE I. Measured (EXP) and calculated (SIM) losses of the plasmofluidic waveguide.

	Propagation loss (dB/μm)/coupling loss (dB)			
w_S (nm)	MISIM	Air	Water	Oil
160 (EXP)	0.33/0.63	1.21/4.14	0.45/2.19	0.50/3.18
160 (SIM)	0.23/0.40	0.17/0.87	0.22/0.53	0.24/0.40
190 (EXP)	0.30/1.03	1.04/6.97	0.59/2.03	0.46/1.79
190 (SIM)	0.21/0.34	0.15/0.75	0.19/0.45	0.21/0.35

This article is copyrighted as indicated in the article. Reuse of AIP content is subject to the terms at: http://scitation.aip.org/termsconditions. Downloaded to IP: 114.70.7.203 On: Wed, 16 Dec 2015 01:14:20

that the reference 450-nm-core waveguide on another chip without the SU-8 microfluidic channel cannot transport sufficient power for measurement due to etching-induced loss. In addition, as shown in Fig. 3(g), the propagation loss for $w_S = 190\,\text{nm}$ is almost proportional to $(n_{\text{Si}}^2 - n_l^2)$, where n_{Si} is the refractive index of Si. This relation is very similar to that observed from the sidewall-roughness-induced propagation loss of a slab waveguide, which is analytically expressed in Ref. 28. Therefore, the sidewall roughness may be the main cause of the propagation loss increase. Although the propagation loss of the plasmofluidic waveguide for $n_l \geq 1.440$ is larger than that of our MISIM waveguide, it is still smaller than those of other MISIM waveguides.[20,21] Considered from a different point of view, the dependence of the propagation loss on n_l indirectly demonstrates that the 30-nm-wide channels are filled with the fluids. This can be confirmed from simulation of the plasmofluidic waveguide with $w_S = 190\,\text{nm}$ for fictitious fluid with $n_l = 1.44 + i0.005$. As shown in the inset of Fig. 4, it is assumed that there is an air gap of height h_A in the channel. The real part of the effective index and propagation loss of the plasmofluidic waveguide are shown with respect to h_A in Fig. 4. The propagation loss significantly decreases from 0.38 to 0.20 dB/μm as h_A increases from 0 to 260 nm. If the fluid covers just the surface of the plasmofluidic waveguide (i.e., $h_A = 260\,\text{nm}$), the propagation loss is slightly larger than that of the air-filled plasmofluidic waveguide (0.15 dB/μm). Therefore, the observed propagation loss change depending on n_l, which is quite large, indicates that the channels are, at least to some extent, filled with the fluids. In the case of the index oil, there is a chance that the channels are partially filled. This is observed in a plasmofluidic disk resonator coupled to the plasmofluidic waveguide, which will be reported elsewhere.

The measured coupling loss also decreases as n_l increases. However, it is quite larger than the calculated coupling loss although the difference between the measured and calculated coupling losses of the MISIM waveguide before the etching process is small. The increase in the measured coupling loss is partly attributed to the sidewall roughness in

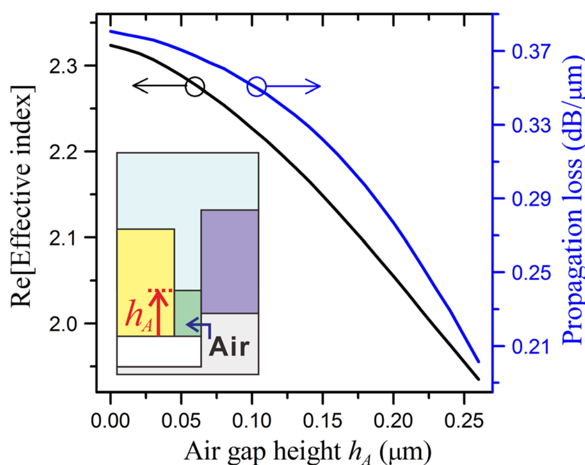

FIG. 4. Calculated real part of the effective index and propagation loss of the plasmofluidic waveguide with $w_S = 190\,\text{nm}$. The inset shows that an air gap of height h_A exists in the channel. The refractive index of the fluid is assumed to be $1.44 + i0.005$.

the tapering region. Other possible causes of the increase may be imperfections in the realized plasmofluidic waveguide such as the bumpy band and the dents in the Cu patterns at the position where the 450-nm-core waveguide is connected to the tapering region. The calculated increase caused by the imperfections is very small ($\leq$0.3 dB). A critical reason for the increase still needs to be found. We also need to improve the fabrication process to minimize the sidewall roughness and the imperfections such that the propagation loss and the coupling loss are reduced.

As mentioned above, the plasmofluidic waveguide is promising as a waveguide device with dynamically tunable phase. The phase of the plasmofluidic waveguide can be either microfluidically tuned by replacing one fluid with another one or electrically tuned by using nematic LC as fluid. It may be challenging but possible to fill the channels with LC since it was experimentally demonstrated that cylindrical channels with diameters smaller than 10 nm are filled with LCs by spontaneous imbibition.[29] In such a LC-filled plasmofluidic waveguide, the Cu patterns are not only used to guide the hybrid plasmonic mode but also used as electrodes. When LC molecules fill the channels, they are expected to be aligned parallel to the channel surfaces.[30–32] Without voltage applied to the electrodes, the ordinary refractive index n_o of the LC molecules mainly affects the dominant electric field component E_x of the hybrid plasmonic mode. When sufficiently large voltage is applied to the electrodes, the LC molecules are almost perfectly aligned perpendicular to the channel surfaces. Then, their extraordinary refractive index n_e mainly affects E_x. The ordinary and extraordinary refractive indices of frequently used LC E7 are 1.50 and 1.68 at $\lambda = 1550\,\text{nm}$, respectively.[33] If the LC is treated as uniform anisotropic fluid, n_l becomes a diagonal matrix with diagonal elements n_{xx}, n_{yy}, and n_{zz}: $n_{xx} = n_{zz} = n_o$ and $n_{yy} = n_e$ without the applied voltage; $n_{yy} = n_{zz} = n_o$ and $n_{xx} = n_e$ with the applied voltage. The real part of the calculated effective index of the hybrid plasmonic mode increases from 2.381 up to 2.533 as the voltage increases; its propagation loss slightly increases from 0.22 to 0.24 dB/μm. The maximum achievable phase change per unit length is $0.20\pi/\mu$m, which is more than two times larger than those calculated for Si strip-loaded slot waveguides ($\leq 0.1\pi/\mu$m).[30] The almost perfect alignment perpendicular to the channel surfaces may be achieved if the potential difference between the Cu pattern and the Si strip is a few volts.[30–32] Then, the voltage across the Cu patterns is estimated by approximating the plasmofluidic waveguide into a parallel plate capacitor. It is roughly $[2 + w_S/(30\,\text{nm})]$ times larger than the potential difference. To make the voltage small, it is necessary to dope the Si strip and use it as a ground electrode. In this way, the LC-filled plasmofluidic waveguide may open the door to an ultracompact phase-tunable device controlled by low driving voltage.

In summary, the plasmofluidic waveguide has been experimentally and theoretically investigated. It is based on the MISIM waveguide which is a hybrid plasmonic waveguide. The insulator of the MISIM waveguide is replaced by fluid, and light is strongly confined in the fluid such that the interaction between the light and the fluid is highly enhanced. The plasmofluidic waveguide has been realized by using the fabrication process based on standard CMOS

This article is copyrighted as indicated in the article. Reuse of AIP content is subject to the terms at: http://scitation.aip.org/termsconditions. Downloaded to IP: 114.70.7.203 On: Wed, 16 Dec 2015 01:14:20

technology. For $w_S = 190$ nm, its measured propagation loss decreases from 1.04 to 0.46 dB/μm as n_l increases from 1 to 1.440. The measured coupling loss between the silicon waveguide with the 450-nm-wide core and the plasmofluidic waveguide also decreases from 6.97 to 1.79 dB. The sidewall roughness and imperfections of the realized plasmofluidic waveguide are considered to make the measured losses larger than the calculated losses. The plasmofluidic waveguide may be used as an optical device trapping nanoparticles as well as a dynamically phase-tunable device.

This research was supported by Basic Science Research Program through the National Research Foundation of Korea (NRF) funded by the Ministry of Education (NRF-2013R1A1A2A10062227) and by the 2015 Research Fund (1.150123) of UNIST (Ulsan National Institute of Science and Technology).

[1]G. Veronis and S. Fan, J. Lightwave Technol. **25**, 2511 (2007).
[2]A. Melikyan, L. Alloatti, A. Muslija, D. Hillerkuss, P. C. Schindler, J. Li, R. Palmer, D. Korn, S. Muehlbrandt, D. V. Thourhout, B. Chen, R. Dinu, M. Sommer, C. Koos, M. Kohl, W. Freude, and J. Leuthold, Nat. Photonics **8**, 229 (2014).
[3]H. W. Lee, G. Papadakis, S. P. Burgos, K. Chander, A. Kriesch, R. Pala, U. Peschel, and H. A. Atwater, Nano Lett. **14**, 6463 (2014).
[4]K. Liu, C. R. Ye, S. Kahn, and V. J. Sorger, Laser Photonics Rev. **9**, 172 (2015).
[5]D. Dai and S. He, Opt. Express **17**, 16646 (2009).
[6]M. Z. Alam, J. Meier, J. S. Aitchison, and M. Mojahedi, Opt. Express **18**, 12971 (2010).
[7]M. Wu, Z. Han, and V. Van, Opt. Express **18**, 11728 (2010).
[8]I. Goykhman, B. Desiatov, and U. Levy, Appl. Phys. Lett. **97**, 141106 (2010).
[9]L. Gao, L. Tang, F. Hu, R. Guo, X. Wang, and Z. Zhou, Opt. Express **20**, 11487 (2012).
[10]N. Zhu and T. Mei, Opt. Lett. **37**, 1751 (2012).
[11]D. A. Ketzaki, O. Tsilipakos, T. V. Yioultsis, and E. E. Kriezis, J. Appl. Phys. **114**, 113107 (2013).
[12]M. P. Nielsen and A. Y. Elezzabi, Appl. Phys. Lett. **103**, 051107 (2013).
[13]N.-N. Feng, M. L. Brongersma, and L. Dal Negro, IEEE J. Quantum Electron. **43**, 479 (2007).
[14]D. Dai and S. He, Opt. Express **18**, 17958 (2010).
[15]X. Sun, L. Zhou, X. Li, Z. Hong, and J. Chen, Appl. Opt. **50**, 3428 (2011).
[16]R. Thomas, Z. Ikonić, and R. W. Kelsall, IEEE J. Sel. Top. Quantum Electron. **19**, 4601708 (2013).
[17]M. P. Nielsen and A. Y. Elezzabi, Opt. Express **21**, 20274 (2013).
[18]S. Zhu, G. Q. Lo, and D. L. Kwong, Appl. Phys. Lett. **99**, 031112 (2011).
[19]S. Zhu, G. Q. Lo, and D. L. Kwong, IEEE Photonics Technol. Lett. **23**, 1896 (2011).
[20]M. P. Nielsen, A. Ashfar, K. Cadien, and A. Y. Elezzabi, Opt. Mater. **36**, 294 (2013).
[21]S. Zhu, G. Q. Lo, and D. L. Kwong, Opt. Express **21**, 8320 (2013).
[22]M.-S. Kwon, Opt. Express **19**, 8379 (2011).
[23]M.-S. Kwon, J.-S. Shin, S.-Y. Shin, and W.-G. Lee, Opt. Express **20**, 21875 (2012).
[24]M.-S. Kwon and J.-S. Shin, Opt. Lett. **39**, 715 (2014).
[25]Y. Fainman, L. P. Lee, D. Psaltis, and C. Yang, *Optofluidics: Fundamentals, Devices, and Applications* (McGraw-Hil, New York, 2009), p. 59.
[26]O. Krupin, H. Asiri, C. Wang, R. N. Tait, and P. Berini, Opt. Express **21**, 698 (2013).
[27]H. S. Lee, C. Awada, S. Boutami, F. Charra, L. Douillard, and R. E. de Lamaestre, Opt. Express **20**, 8974 (2012).
[28]F. Grillot, L. Vivien, S. Laval, D. Pascal, and E. Cassan, IEEE Photonics Technol. Lett. **16**, 1661 (2004).
[29]S. Calus, D. Rau, P. Huber, and A. V. Kityk, Phys. Rev. E **86**, 021701 (2012).
[30]J. Pfeifle, L. Alloatti, W. Freude, J. Leuthold, and C. Koos, Opt. Express **20**, 15359 (2012).
[31]D. C. Zografopoulos and R. Beccherelli, J. Opt. **15**, 055009 (2013).
[32]Y. Xing, T. Ako, J. P. George, D. Korn, H. Yu, P. Verheyen, M. Pantouvaki, G. Lepage, P. Absil, A. Ruocco, C. Koos, J. Leuhold, K. Neyts, J. Beeckman, and W. Bogaerts, IEEE Photonics Technol. Lett. **27**, 1269 (2015).
[33]D.-P. Cai, S.-C. Nien, H.-K. Chiu, C.-C. Chen, and C. Chieh, Opt. Express **19**, 11890 (2011).

This article is copyrighted as indicated in the article. Reuse of AIP content is subject to the terms at: http://scitation.aip.org/termsconditions. Downloaded to IP: 114.70.7.203 On: Wed, 16 Dec 2015 01:14:20